

Anticancer activity of two ruthenium(II) polypyridyl complexes toward Hepatocellular carcinoma HepG-2 cells

Guang-Bin Jiang^{a,*}, Wen-Yao Zhang^b, Miao He^b, Yi-Ying Gu^b, Lan Bai^b, Yang-Jie Wang^b, Qiao-Yan Yi^b, Fan Du^b

^a Guangxi Key Laboratory of Electrochemical and Magneto-chemical Function Materials, College of Chemistry and Bioengineering, Guilin University of Technology, Guilin 541004, China

^b School of Pharmacy, Guangdong Pharmaceutical University, Guangzhou 510006, China

ARTICLE INFO

Article history:

Received 10 March 2019

Accepted 9 May 2019

Available online 18 May 2019

Keywords:

Ruthenium(II) polypyridyl complex

DNA binding

Reactive oxygen species

Cell invasion

Mitochondrial membrane potentials

ABSTRACT

Two novel ruthenium(II) polypyridyl complexes $[\text{Ru}(\text{bpy})_2(\text{ETPIP})](\text{ClO}_4)_2$ (**Ru(II)-1**) and $[\text{Ru}(\text{phen})_2(\text{ETPIP})](\text{ClO}_4)_2$ (**Ru(II)-2**) (bpy = 2,2'-bipyridine, ETPIP = 2-(4-(thiophen-2-ylethynyl)phenyl)-1H-imidazo[4,5-f][1,10]phenanthroline, phen = 1,10-phenanthroline) have been synthesized and characterized. The DNA binding behaviors were evaluated using electronic absorption titration, luminescence spectra and viscosity measurement, revealing an intercalative mode. The cytotoxicity of the ligand and Ru(II) complexes toward A549, HepG-2, SGC-7901 and Hela was assayed by MTT ((3-(4,5-dimethylthiazo-2-yl)-2,5-diphenyltetrazolium bromide)) method. Notably, ETPIP shows no anticancer activity against selected cell lines, and complexes **Ru(II)-1** ($\text{IC}_{50} = 18.4 \pm 2.1 \mu\text{M}$) and **Ru(II)-2** ($\text{IC}_{50} = 16.5 \pm 1.7 \mu\text{M}$) were found to be slightly more effective against HepG-2 cells than cisplatin ($\text{IC}_{50} = 26.4 \pm 2.6 \mu\text{M}$). Evaluation of cell invasion was performed with the Boyden chamber invasion assay. Additionally, the cell cycle distribution of HepG-2 cells was carried out by flow cytometry. Most importantly, the further anticancer mechanism of the Ru(II) complexes was explored by apoptosis, intracellular reactive oxygen species (ROS) levels and mitochondrial membrane potentials. These results reveal that complexes **Ru(II)-1** and **Ru(II)-2** could induce apoptosis in HepG-2 cells via a ROS-mediated mitochondrial dysfunction pathway.

© 2019 Elsevier Ltd. All rights reserved.

1. Introduction

The discovery of cisplatin as anticancer drug by Rosenberg et al. opens the new pathway for cancer chemotherapy [1,2]. To date, cisplatin and its analogues are some of the more effective chemotherapeutic drugs in clinical use [3–5]. However, even though the treatment of various malignant cancers with cisplatin is quite successful, this comes at the price of serious side effects such as nephrotoxicity, myelotoxicity, neural damage, and ototoxicity which limit its clinical applicability [6,7]. Therefore, obtaining other metal-based anticancer agents, which could broaden the spectrum of anti-tumors, reduce the occurrence of side effects, and overcome platinum resistance, has attracted widespread attention [8,9]. It was believed that the complexes containing ruthenium exhibit low toxicity, easily absorbed and rapidly excreted by the body, and will become one of the most promising anti-cancer drugs [10–23]. In recent years, the studies of the ruthenium

polypyridyl complexes on the anticancer field have made significant progress. It has been reported that $[\text{Ru}(\text{phen})_2(\text{MHPIP})](\text{ClO}_4)_2$ (phen = 1,10-phenanthroline) can effectively inhibit the proliferation of HepG-2 cells by inducing apoptotic cell death through ROS-mediated mitochondrial dysfunction pathways [24]. Xu and co-workers first reported that $[\text{Ru}(\text{N-N})_2-(1\text{-Py}-\beta\text{C})](\text{PF}_6)_2$ (N-N = 2,2'-bipyridine (bpy); 1,10-phenanthroline (phen), 4,7-diphenyl-1,10-phenanthroline (DIP); 1-Py-βC = 1-(2-pyridyl)-β-carboline) can induce apoptosis and autophagy simultaneously in Hela cells through a ROS mediated mechanism [25]. Very recently, Ru(II) complex $[(\text{piq})\text{Ru}(\text{bpy})_2]^{2+}$ (piq = phenylisoquinolate, bpy = 2,2'-bipyridine) shows high inhibition of cell growth toward MDA-MB-231 cells [26]. It is worth to mention that two ruthenium-based complexes, NAMI-A and KP1019 have entered clinical trials [27,28].

The incorporation of heterocycle can partially modify the biological properties of the parent molecules, thus heterocycle containing compounds are significant oriented targets in medicinal chemistry. In this report, a thiophene-containing ligand ETPIP (ETPIP = 2-(4-(thiophen-2-ylethynyl)phenyl)-1H-imidazo

* Corresponding author. Fax: +86 773 899 1304.

E-mail address: jianggb@glut.edu.cn (G.-B. Jiang).

[4,5-*f*][1,10]phenanthroline) and its two ruthenium(II) polypyridyl complexes $[\text{Ru}(\text{bpy})_2(\text{ETPIP})](\text{ClO}_4)_2$ (**Ru(II)-1**) and $[\text{Ru}(\text{phen})_2(\text{ETPIP})](\text{ClO}_4)_2$ (**Ru(II)-2**) (Scheme 1) were synthesized and characterized by ^1H NMR, ^{13}C NMR, HRMS and IR. To the best of our knowledge, this form of ETPIP-containing Ru(II) complexes is used for the first time as anticancer agents. The interaction of the two ruthenium(II) polypyridyl complexes with calf thymus (CT DNA) was investigated via electronic absorption titration, viscosity measurements and luminescence spectra. The cytotoxicity of the ligand and Ru(II) complexes toward A549, HepG-2, SGC-7901 and HeLa were detected by MTT ((3-(4,5-dimethylthiazo-2-yl)-2,5-diphenyl-tetrazolium bromide)) method. In addition, the possible anticancer mechanism of the ruthenium(II) polypyridyl complexes was explored by apoptosis, intracellular reactive oxygen species (ROS) levels, cell invasion assay, cell cycle arrest, mitochondrial membrane potentials and location in mitochondria. All these results point out that these thiophene-containing Ru(II) complexes possess excellent anticancer activity that make them attractive as a potentially promising candidate for the development of anticancer agents.

2. Experimental

2.1. Materials and methods

All reagents and solvents were purchased commercially and used without further purification unless otherwise noted. Calf thymus DNA (CT DNA) was obtained from the Sino American Biotechnology Company. Ltd. Ultrapure MilliQ water was used in all experiments. DMSO and RPMI 1640 were purchased from Sigma. Cell lines of HeLa (Human cervical cancer cell line), SGC-7901 (human gastric carcinoma cells), HepG-2 (Hepatocellular carcinoma cells) and A549 (Human lung carcinoma cells) were purchased from the American Type Culture Collection. $\text{RuCl}_3 \cdot 3\text{H}_2\text{O}$ was obtained from the Kunming Institution of Precious Metals. 2,2'-Bipyridine and 1,10-phenanthroline were obtained from the Guangzhou Chemical Reagent Factory.

Analytical thin layer chromatography was performed by using commercially prepared 100–400 mesh silica gel plates (GF_{254}) and visualization was effected at 254 nm. Mass spectra were recorded on a Thermo Scientific ISQ gas chromatograph-mass spectrometer. The data of HRMS was carried out on a high-resolution mass spectrometer (LCMS-IT-TOF). IR spectra were obtained either as potassium bromide pellets or as liquid films between two potassium bromide pellets with a Bruker TENSOR 27 spectrometer. ^1H NMR spectra were recorded on a Varian-500 spectrometer with $\text{DMSO}-d_6$ as solvent and tetramethylsilane (TMS) as an internal standard at 400 MHz at room temperature.

2.2. Synthesis of ligand and complexes

2.2.1. Synthesis of 4-(thiophen-2-ylethynyl)benzaldehyde

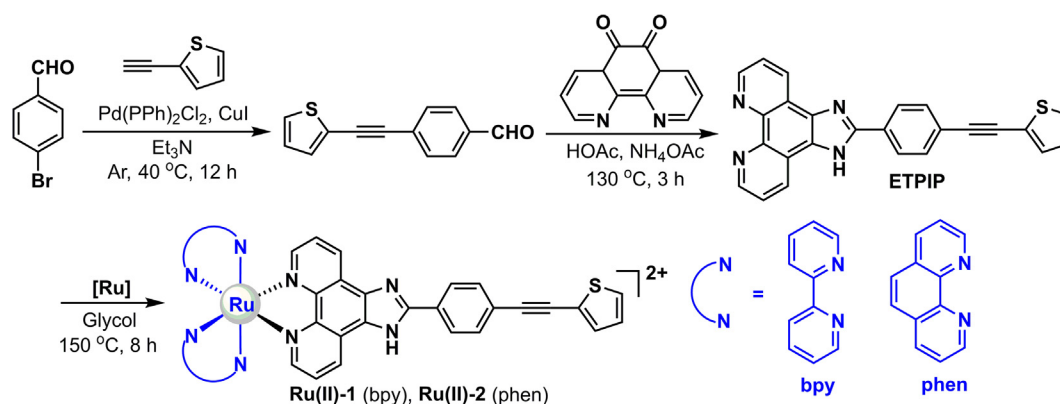
To a resealable Schlenk tube or alternatively, a screw-cap pressure tube, were added 4-bromobenzaldehyde (1.0 mmol, 1.0 equiv), CuI (10 mol %), $\text{Pd}(\text{PPh}_3)_2\text{Cl}_2$ (5 mol%), 2-ethynylthiophene (1.3 mmol, 1.3 equiv), Et_3N (8 mL) and a stir bar. The reaction vessel was fitted with a rubber septum, and was evacuated and back-filled with nitrogen. The reaction tube was sealed and immersed in a preheated oil bath at 40°C for 12 h and the solution was stirred with the aid of a magnetic stirrer. After attaining ambient temperature, the reaction mixture was diluted with ethyl acetate and filtered through a plug of silica gel. The filtrate was concentrated and the resulting residue was purified by column chromatography (silica gel, petroleum ether/ EtOAc) to give the desired substrates.

2.2.2. Synthesis of ligand (ETPIP)

A mixture of 1,10-phenanthroline-5,6-dione (100 mg, 0.500 mmol), 4-(thiophen-2-ylethynyl)benzaldehyde (106 mg, 0.500 mmol), ammonium acetate (15 mmol, 1156.2 mg) and acetic acid (30 mL) was refluxed with stirring for 4 h. The cooled solution was diluted with water and neutralized with concentrated aqueous ammonia. The brown precipitate was collected and purified by column chromatography on silica gel (60 ~ 100 mesh) with ethanol as eluent to give the compound as a brown yellow powder. Yield: 338.0 mg, 84%. ^1H NMR (400 MHz, $\text{DMSO}-d_6$) δ 9.02 (s, 2H), 8.91 (d, $J = 7.7$ Hz, 2H), 8.33 (d, $J = 7.7$ Hz, 2H), 7.95 (s, 1H), 7.80 (dd, $J = 7.1, 3.9$ Hz, 2H), 7.76–7.66 (m, 3H), 7.32 (d, $J = 4.7$ Hz, 1H); IR: $\nu = 3099, 2202, 1887, 1692, 1603, 1555, 1470, 1440, 1400, 1357, 1194, 1120, 943, 835, 733, 616$ cm^{-1} ; HRMS (ESI) m/z : calcd for $\text{C}_{25}\text{H}_{15}\text{N}_4\text{S}$ $[\text{M}+\text{H}]^+$, 403.1012; found 403.1017.

2.2.3. Synthesis of $[\text{Ru}(\text{bpy})_2(\text{ETPIP})](\text{ClO}_4)_2$ (**Ru(II)-1**)

A mixture of *cis*- $[\text{Ru}(\text{bpy})_2\text{Cl}_2] \cdot 2\text{H}_2\text{O}$ (158.7 mg, 0.3 mmol) and ETPIP (120.6 mg, 0.3 mmol) in ethylene glycol (12 mL) was heated at 150°C under argon for 8 h to give a clear red solution. Upon cooling, a red precipitate was obtained by dropwise addition of saturated aqueous NaClO_4 solution. The crude product was purified by column chromatography on neutral alumina with a mixture of CH_3CN -toluene (1:1, v/v) as eluent. The red band was collected. The solvent was removed under reduced pressure and a red powder was obtained. Yield: 224.5 mg, 73%. ^1H NMR (400 MHz, $\text{DMSO}-d_6$) δ 8.97 (d, $J = 63.5$ Hz, 6H), 8.20 (dd, $J = 77.3, 35.0$ Hz, 8H), 7.81 (d, $J = 86.1$ Hz, 12H), 7.36 (d, $J = 41.7$ Hz, 4H); ^{13}C NMR (100 MHz, $\text{DMSO}-d_6$) δ 157.3, 157.1, 151.9, 149.9, 149.9, 145.4, 138.4, 138.3, 132.3, 130.9, 130.8, 130.8, 130.1, 128.4, 128.2, 127.6, 127.2, 126.6, 124.9, 124.9, 124.3, 123.9, 123.9, 121.5, 119.7, 89.0, 87.2;



Scheme 1. The synthetic route of ligand and ruthenium complexes.

IR: $\nu = 3074, 1602, 1512, 1477, 1463, 1446, 1271, 1244, 1199, 1093, 843, 806, 766, 742, 729, 624 \text{ cm}^{-1}$; HRMS (ESI) m/z : calcd for $\text{C}_{45}\text{-H}_{29}\text{N}_8\text{RuS} [\text{M}-2\text{ClO}_4\text{-H}]^+$, 815.1285; found 815.1291.

2.2.4. Synthesis of $[\text{Ru}(\text{phen})_2(\text{ETPIP})](\text{ClO}_4)_2$ (**Ru(II)-2**)

This complex was synthesized in an identical manner to that described for complex **Ru(II)-1**, with *cis*- $[\text{Ru}(\text{phen})_2\text{Cl}_2]\cdot 2\text{H}_2\text{O}$ [23,29]. In place of *cis*- $[\text{Ru}(\text{bpy})_2\text{Cl}_2]\cdot 2\text{H}_2\text{O}$. Yield: 254.3 mg, 79%. ^1H NMR (400 MHz, $\text{DMSO}-d_6$) δ 8.97 (d, $J = 7.5 \text{ Hz}$, 2H), 8.78 (d, $J = 7.8 \text{ Hz}$, 4H), 8.40 (s, 4H), 8.31 (d, $J = 7.2 \text{ Hz}$, 2H), 8.18 (dd, $J = 26.7, 3.0 \text{ Hz}$, 4H), 8.00 (s, 2H), 7.90 (s, 1H), 7.84–7.70 (m, 6H), 7.65 (d, $J = 6.8 \text{ Hz}$, 3H), 7.28 (s, 1H); ^{13}C NMR (100 MHz, $\text{DMSO}-d_6$) δ 153.9, 153.2, 153.1, 150.2, 147.8, 145.7, 137.3, 135.7, 134.0, 132.3, 132.2, 131.1, 131.0, 130.8, 130.7, 130.1, 128.5, 127.6, 127.1, 126.8, 126.8, 126.4, 126.3, 124.4, 124.4, 123.7, 121.5, 89.0, 87.2; IR: $\nu = 3066, 1601, 1576, 1511, 1478, 1361, 1250, 1200, 1092, 843, 804, 740, 721, 697, 624 \text{ cm}^{-1}$; HRMS (ESI) m/z : calcd for $\text{C}_{49}\text{H}_{29}\text{N}_8\text{RuS} [\text{M}-2\text{ClO}_4\text{-H}]^+$, 863.1286; found 863.1289.

Caution: Perchlorate salts of metal compounds with organic ligands are potentially explosive, and only small amounts of the material should be prepared and handled with great care.

2.3. Ruthenium(II) complexes–CT–DNA binding

The absorption spectra of target complexes were collected in the presence of increasing concentration of calf thymus DNA (CT DNA). Stock solutions of target complexes were made by dissolution of the complexes in dimethyl sulfoxide and diluting to a required concentration using a buffer [5 mM Tris–HCl, 50 mM NaCl, pH 7.0]. The concentration of DNA was calculated using the molar extinction coefficient of $6600 \text{ M}^{-1} \text{ cm}^{-1}$ at 260 nm [30]. DNA was added to both the sample cuvette and the reference cuvette. After the DNA was allowed to equilibrate with the complex solution for 5 min, the spectra were measured [31]. The absorption titrations of the complex in buffer were performed using a fixed concentration ($5.0 \mu\text{M}$) for complex to which increments of the DNA stock solution were added. The intrinsic-binding constant K_b was calculated according to the following equation:

$$[\text{DNA}]/(\varepsilon_a - \varepsilon_f) = [\text{DNA}]/(\varepsilon_b - \varepsilon_f) + 1/[K_b(\varepsilon_b - \varepsilon_f)]$$

In this equation, [DNA] is the concentration of DNA added, while ε_a , ε_f and ε_b corresponds to the apparent molar absorptivity, the molar absorptivity for the free complex [32], and the molar absorptivity for the complex when saturated, respectively.

The viscosity of a DNA solution was measured in the presence of increasing amounts of complexes **Ru(II)-1** and **Ru(II)-2**. The flow time was measured with a digital stopwatch, each sample was measured at least five times, and then the average flow time was calculated [33]. Relative viscosities for DNA in the presence and absence of target complexes were calculated from the relation $\eta = (t - t^0)/t^0$, where t is the observed flow time of the DNA-containing solution and t^0 is the flow time of buffer alone [34,35]. The change in the viscosity was presented as $(\eta/\eta_0)^{1/3}$ versus binding ratio $[\text{Ru}]/[\text{DNA}]$ [36], where η is the viscosity of DNA solution in the presence of complexes and η_0 is the viscosity of DNA solution alone.

2.4. Cytotoxicity assay in vitro

Cytotoxic effect of the complexes against selected tumor cell lines were determined by a rapid colorimetric assay, using MTT (3-(4,5-dimethyl thiazol-2-yl)-2,5-diphenyl tetrazolium bromide) [37]. This assay is based on the metabolic reduction of soluble MTT by mitochondrial enzyme activity of viable cells into an insol-

uble colored formazan product, which can be measured spectrophotometrically after dissolving in DMSO. Cells were seeded in 96-well plates with 8000 cells/well and divided into control and treatment group. The tested complexes were then added to the wells to achieve final concentrations ranging from 10^{-6} to 10^{-4} M . Control wells were prepared by addition of culture medium (100 μL). After 48 h incubation, culture medium was removed and cells were washed using PBS. 5 mg/mL of MTT was diluted by PBS (1 mL MTT stock add 10 mL PBS) and 100 μL of it was added into every well. Then, the plate was incubated for 4 h until formazan was produced. The purple-blue formazan precipitate was dissolved in 100 μL of DMSO and the absorbance values were determined at 490 nm by a multi-well plate reader. Data obtained from at least three separate experiments, while there were untreated and DMSO treated cells as negative and positive controls, respectively.

2.5. Apoptosis assessment by AO/EB staining

Acridine orange (AO) and ethidium bromide (EB) staining method was carried out to evaluate morphological evidence of apoptosis on the treated cells. Briefly, 2×10^5 HepG-2 cells were seeded on chamber slides in a 12-well plate and allowed to attach overnight and the cells were treated with ruthenium(II) complexes ($8.5 \mu\text{M}$). After the treatment (24 h), the HepG-2 cells were counterstained with acridine orange (AO) and ethidium bromide (EB) (AO: $100 \mu\text{g mL}^{-1}$, EB: $100 \mu\text{g mL}^{-1}$) and incubated for 10 min. The unbound dye was removed by washing with PBS and the cells were fixed with methanol and glacial acetic acid (3:1) for 1 h at room temperature. The nuclear morphology of the cells was observed and imaged with a fluorescence microscope (Nikon, Yokohama, Japan).

2.6. Apoptosis assay by flow cytometry

Induction of apoptosis was studied by Annexin V-FITC and Propidium iodide (PI) binding assay. HepG-2 cells (6×10^5) were treated with different concentration ($8.5 \mu\text{M}$ and $16.5 \mu\text{M}$) of ruthenium(II) complexes at 37°C for 24 h to quantify normal and apoptosis HepG-2 cells. After treatment, cells were trypsinized and resuspended in original media to include the dead cells and washed with PBS. Cells were pelleted and resuspended in 1X media binding buffer and then labelled with Annexin V-FITC and propidium iodide (PI) according to manufacturer's instructions followed by incubation for 30 min in the dark. The fluorescence intensities of the cells of each of the three batches were examined in triplicates by FACS Caliber flow cytometer (Beckman Dickinson & Co., Franklin Lakes, NJ). A minimum of 10,000 cells were analyzed per sample. A minimum of 10,000 cells were analyzed per sample. The fluorescence of cell population and the acquisition was then performed using FlowJo software.

2.7. Reactive oxygen species (ROS) levels studies

For measuring the total ROS level, HepG-2 cells were seeded in a 12-well plate and allowed to attach overnight. Medium was replaced with fresh medium, cells were treated with ruthenium (II) complexes and allowed to incubate for 24 h. After treatment, the cells were washed twice with cold PBS and subsequently pre-stained with DCFH-DA (10 mM) and incubated at 37°C in the dark for 30 min. Finally, the cells were washed with $3 \times$ PBS, and then imaged and quantitatively analyzed using a confocal fluorescence microscope.

2.8. The change of mitochondrial membrane potential assay

The HepG-2 cells were seeded in 12-well plates at a density of 2×10^5 cells/mL, and the $IC_{50}/2$ doses of **Ru(II)-1** and **Ru(II)-2** were added to cells. The cells were incubated in 5% CO_2 air-conditioned atmosphere at 37 °C. After 24 h of incubation, the cells were washed two times with PBS. Subsequently, JC-1 dye (1 μ g/mL) was added and incubated for 20 min in the dark at 37 °C. After being washed with PBS, the cells were covered with PBS, and observed under an ImageXpress Micro XLS system.

2.9. Location assay of the complex in the mitochondria

HepG-2 cells were seeded in 12-well plates at 2×10^5 cells/well and incubated for 24 h at 37 °C and 5% CO_2 . After that, 1.0 μ M of the complexes were added to the wells at 37 °C in a 5% CO_2 incubator for 4 h and further co-incubated with MitoTracker[®] Deep Green FM (150 nM) at 37 °C for 0.5 h. Upon completion of the incubation, the wells were washed three times with ice-cold PBS. After discarding the culture medium, the cells were imaged under an ImageXpress Micro XLS system.

2.10. Matrigel invasion assay

For the cell invasion assays, Matrigel (BD Biosciences) was thawed on ice at 4 °C overnight and diluted with serum-free medium at a ratio of 1:3. Then, the Transwell chambers were coated with 30 μ L diluted Matrigel in a 24-well plate and incubated at 37 °C for 4 h. Subsequently, 1.5×10^5 HepG-2 cells in serum-free RPMI-1640 containing the indicated concentration of ruthenium (II) complexes were seeded into the prepared Transwell chambers. Afterward, 400 μ L RPMI-1640 with 20% FBS and the indicated concentration of ruthenium(II) complexes were added to the lower chamber. The 24-well plate was then incubated at 37 °C with 5% CO_2 for 24 h. The cells were fixed and stained as in the migration assay. The membranes were photographed and the invading cells were counted under a light microscope. The mean values from three independent assays were calculated.

2.11. Cell cycle arrest by flow cytometry

HepG-2 cells were seeded in 6-well plates at 3×10^5 cells/well and incubated overnight to allow attachment. The cells were treated with the indicated concentration of the target complexes. After 24 h of incubation, HepG-2 cells were trypsinised and washed with PBS 3 times. The resulting pellet was fixed with 70% ethanol and stored at –20 °C for one day. Fixed cells were washed with PBS, followed by the addition of 50 mg/mL RNase and staining with 50 mg/mL propidium iodide (PI) (Sigma-Aldrich, USA). PI binds DNA as well as RNA. Thus, the addition of RNase enzyme was essential to allow PI to bind RNA directly to obtain an accurate cell-cycle profile. The HepG-2 cells were incubated between 30 min and 60 min at 37 °C. Finally, the cell-cycle kinetics were analysed using a FACS Caliber flow cytometer.

3. Results and discussion

3.1. In vitro cytotoxicity assay

The cytotoxicity of ETPIP and its two Ru(II) complexes (**Ru(II)-1** and **Ru(II)-2**) in vitro were evaluated on four cancer cell lines (A549, HepG-2, SGC-7901 and Hela) using the MTT method assay. The preliminary bioassay results were compared with cisplatin. The activity was expressed as the concentration (IC_{50}) that causes 50% inhibition of cancer cell proliferation and is summarized in

Table 1. As shown in **Table 1**, unsurprisingly, ligand ETPIP is found to display no cytotoxic activity toward the selected tumor cell lines. To our delight, complex **Ru(II)-1** displayed significant and selective cytotoxicities with IC_{50} values lower than 20 μ M against HepG-2 cells. In addition, **Ru(II)-2** exhibited excellent activity against A549, HepG-2, SGC-7901 and Hela with IC_{50} values of 26.1 ± 2.6 , 16.5 ± 1.7 , 28.1 ± 2.6 and 14.9 ± 1.5 μ M, respectively. Most importantly, the anticancer activities of **Ru(II)-1** and **Ru(II)-2** are slightly more effective than that of cisplatin against HepG-2 cells under the identical conditions. The difference in cytotoxic activity of the complexes **Ru(II)-1** and **Ru(II)-2** toward the same tumor cell line may be caused by different ancillary ligands, different ancillary ligands induce different function of complexes [38].

3.2. Apoptosis assay with AO/EB and Annex V/PI double staining methods

Disruption or inappropriate regulation of apoptotic and necrosis processes can result in several diseases including cancer [24]. In order to observe the morphological changes of HepG-2 cells, acridine orange (AO)/ethidium bromide (EB) fluorescent staining assay was conducted to distinguish the live, apoptotic and necrotic cells [39]. In this method, AO, the vital dye, penetrates into both live and dead cells and emits green fluorescence when it binds to double-stranded nucleic acid. Ethidium bromide (EB) provides a red–orange fluorescence by staining fragmented DNA of nuclear membrane ruptured cells [40]. Therefore, the viable cells will be uniformly stained green, apoptotic cells are stained green and contain apoptotic characteristics such as cell blebbing, nuclear shrinkage and chromatin condensation, necrotic cells are stained as red and can be found by the AO/EB double staining [38]. After HepG-2 cells were exposed to 8.5 μ M of different Ru(II) complexes (**Ru(II)-1** and **Ru(II)-2**) for 24 h, the observations are shown in **Fig. 1**. Control cells (a) have shown uniform green cells, which confirm the presence of live cells. The treatment of HepG-2 cells with **Ru(II)-1** (b) and **Ru(II)-2** (c), the apoptotic cells with apoptotic features such as cell blebbing, nuclear shrinkage and chromatin condensation, as well as red necrotic cells, were observed. The observations demonstrated that the complexes **Ru(II)-1** and **Ru(II)-2** can induce apoptosis in HepG-2 cells.

In order to further quantitatively compare the apoptotic effect of the ruthenium(II) complexes, Annex V/PI double staining was employed to determine the percentage of apoptotic cells. As shown in **Fig. 2**, HepG-2 cells treated with different concentrations of complexes **Ru(II)-1** (b, c) and **Ru(II)-2** (d, e) for 24 h, the percentage of apoptotic (Q3) cells was increased to 14.6% for **Ru(II)-1** and 15.1% for **Ru(II)-2** in comparison with the control (a, 2.6%), indicating that the **Ru(II)-1** and **Ru(II)-2** could induce early apoptosis in HepG-2 cells. In addition, the level of apoptosis shows a concentration-dependent manner.

3.3. Location assay of the complexes and mitochondrial membrane potential (MMP) analysis

Disruption and permanent dissipation of the inner mitochondrial membrane potential ($\Delta\Psi_m$) is an event that is associated

Table 1
 IC_{50} (μ M) values of ligand and [Ru] complexes against the selected cancer cell lines.

complex	A549	HepG-2	SGC-7901	Hela
ETPIP	>100	>100	>100	>100
Ru(II)-1	38.0 ± 3.5	18.4 ± 2.1	41.7 ± 4.3	21.0 ± 2.3
Ru(II)-2	26.1 ± 2.6	16.5 ± 1.7	28.1 ± 2.6	14.9 ± 1.5
Cisplatin	8.2 ± 1.4	26.4 ± 2.6	4.4 ± 1.3	8.3 ± 1.1

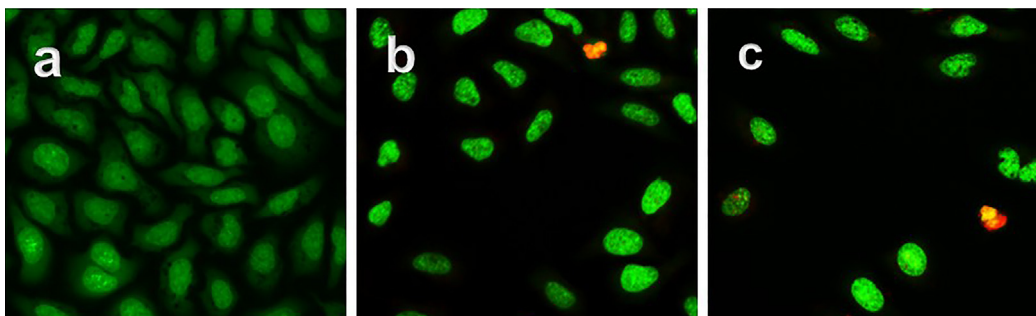


Fig. 1. Apoptosis in HepG-2 cells (a) exposure to 8.5 μM of complexes **Ru(II)-1** (b) and **Ru(II)-2** (c) for 24 h and the cells were stained with AO/EB.

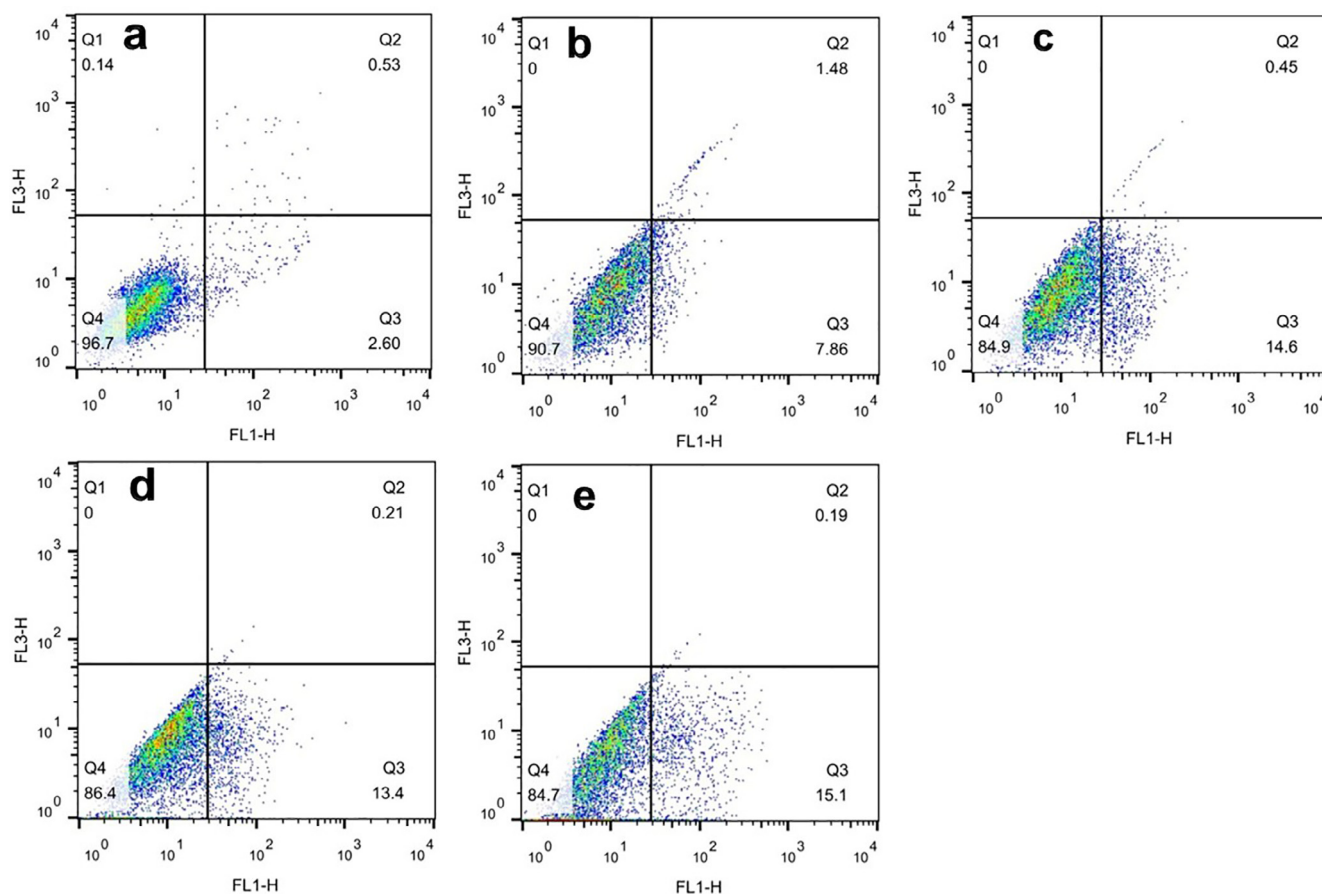


Fig. 2. Apoptosis was assayed with Annex V/PI staining HepG-2 cells (a) in the presence of **Ru(II)-1** (8.5 μM) (b), **Ru(II)-1** (16.5 μM) (c), **Ru(II)-2** (8.5 μM) (d), and **Ru(II)-2** (16.5 μM) (e) for 24 h.

with the intrinsic pathway of apoptosis [41]. Therefore, to further clarify the possible mechanism of apoptosis. The location of the ruthenium(II) polypyridyl complexes in the mitochondria was detected using Mito Tracker[®] Deep Green FM (ThermoFisher, 100 nM) as a green fluorescent dye [42]. As shown in Fig. 3, in the control, the mitochondria were stained in green by Mito Tracker[®] Deep Green. The treatment of HepG-2 cells with 1.0 μM of **Ru(II)-1** and **Ru(II)-2** for 4 h, the complexes emit red fluorescence. The merge of the green and red fluorescence indicates that the ruthenium(II) polypyridyl complexes could arrive the cytoplasm through the cell membrane and accumulate in the mitochondria. To further evaluate the antitumor mechanism. The effects of complexes **Ru(II)-1** and **Ru(II)-2** on the mitochondrial membrane potential of HepG-2 cells was monitored by detecting

the red/green fluorescence of JC-1 by ImageXpress Micro XLS system. JC-1 can be aggregated in a MMP-dependent manner in mitochondria, where green fluorescence indicates a decrease in MMP and red fluorescence means high membrane potentials [43]. As shown in Fig. 4, in the control (a), JC-1 emits red fluorescence corresponding to high MMP. HepG-2 cells were incubated with CCCP (carbonylcyanide-m-chlorophenylhydrazone, b, positive control), **Ru(II)-1** (8.5 μM , c) and **Ru(II)-2** (8.5 μM , d) for 24 h, JC-1 emits green fluorescence corresponding to low MMP. Therefore, the two Ru(II) complexes caused a remarkable decrease in MMP, as evidenced by the fluorescence shift from red to green. Subsequently, the ratios of red/green fluorescent intensity were also determined as shown in Fig. 5. In the control, the ratio of red/green fluorescence is 0.74. Treatment of HepG-2 cells with 16.5 μM of

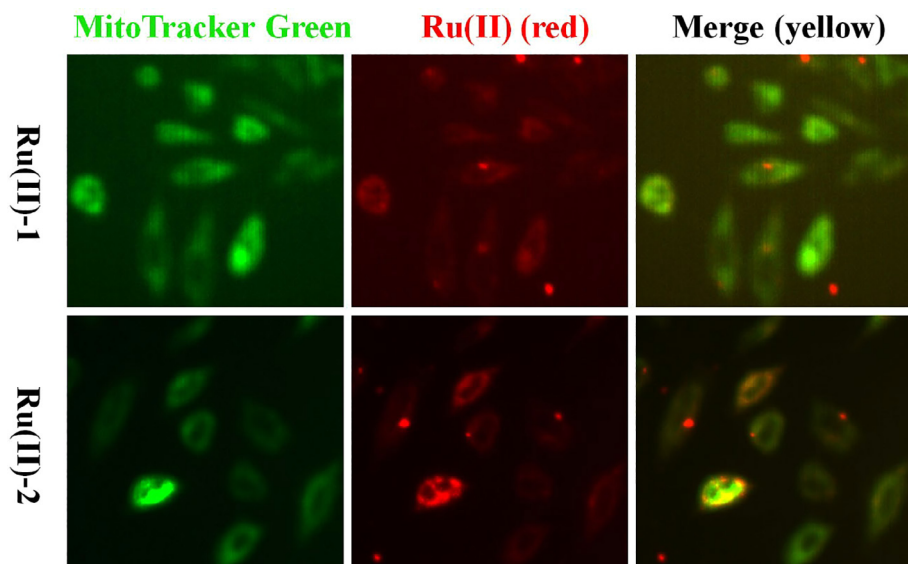


Fig. 3. (A) Location of complexes in the mitochondria in HepG-2 cells exposure to 1.0 μM of complexes **Ru(II)-1** and **Ru(II)-2** for 4 h.

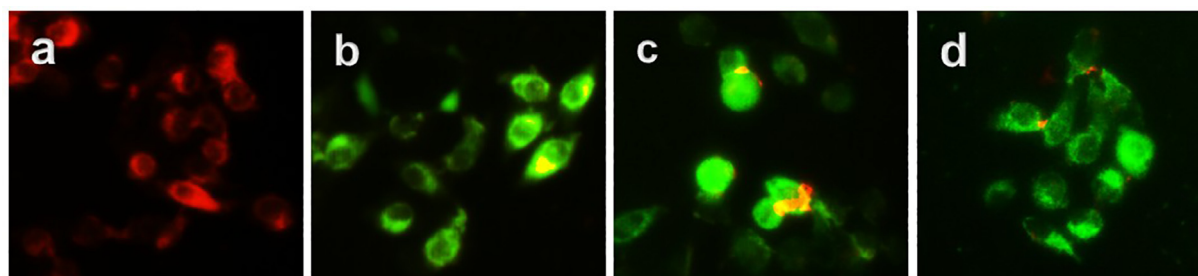


Fig. 4. The changes of mitochondrial membrane potential was studied after HepG-2 cells (a) were treated with CCCP (b), 8.5 μM of complexes **Ru(II)-1** (c) and **Ru(II)-2** (d) for 24 h and the cells were imaged under a fluorescent microscope.

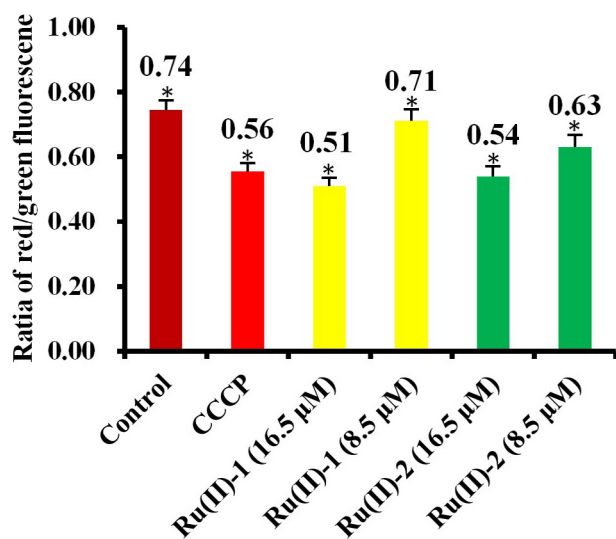


Fig. 5. The ratio of the red/green fluorescent intensity was determined after HepG-2 cells were treated with 8.5 and 16.5 μM of Ru(II) complexes for 24 h. * $P < 0.05$ represents significant differences compared with control. (Color online.)

complexes **Ru(II)-1** and **Ru(II)-2**, the ratios of red/green fluorescence are 0.51 and 0.54, respectively. The decreases of the ratio indicate that the green fluorescent intensities increase and the red fluorescent intensities reduce. In addition, the impairment in

MMP induced by **Ru(II)-1** and **Ru(II)-2** were clearly concentration-dependent in HepG-2 cells.

3.4. Intracellular reactive oxygen species levels determination

Dysfunction of mitochondrial functions, such as the reduction of mitochondrial membrane potential (MMP), may result in over-generation of intracellular reactive oxygen species (ROS) [44]. The ROS generated in cancer cells were monitored using the fluorescent probe 2',7'-dichlorodihydrofluorescein diacetate (DCFH-DA), which could primarily be hydrolyzed and penetrate the cell membrane to form DCFH [45]. DCFH has non-fluorescence and cannot pass through the cell membrane. Then, DCFH can be oxidized by ROS into fluorescent DCF. Therefore, the fluorescence intensity of DCF can reflect the content of intracellular ROS [46]. The DCF fluorescent intensity was tested by ImageXpress Micro XLS system. As shown in Fig. 6, in the control (a), no obvious green fluorescence image was detected. After HepG-2 cells were incubated with Rosup (positive control, b), **Ru(II)-1** (8.5 μM , c) and **Ru(II)-2** (8.5 μM , d) for 24 h, the remarkable fluorescence images were observed. These results indicate that ROS in HepG-2 cells can be generated and complexes (**Ru(II)-1** and **Ru(II)-2**) can increase the contents of ROS. To further quantitatively evaluate the levels of the ROS induced by **Ru(II)-1** and **Ru(II)-2**. The DCF fluorescent intensity was tested by ImageXpress Micro XLS system. As shown in Fig. 7, in the control, the DCF fluorescent intensity is 8.6. However, HepG-2 cells were treated with 16.5 μM of complexes

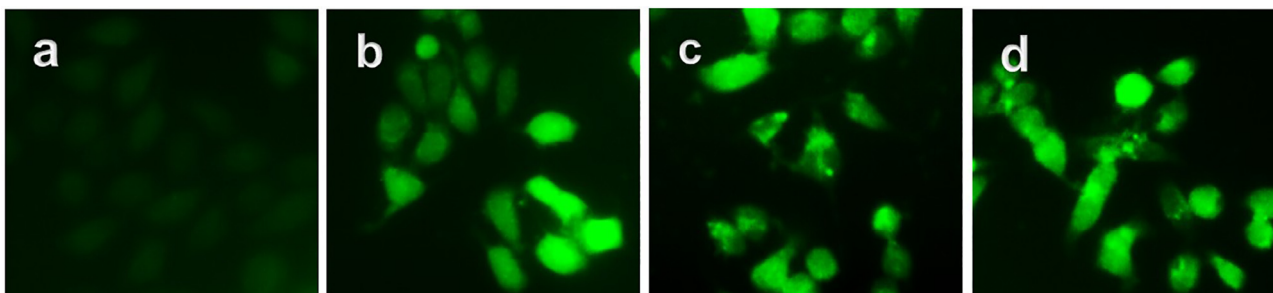


Fig. 6. Intracellular ROS was detected in HepG-2 cells (a) exposure to Rosup (b, positive control), 8.5 μM of **Ru(II)-1** (c) and **Ru(II)-2** (d) for 24 h.

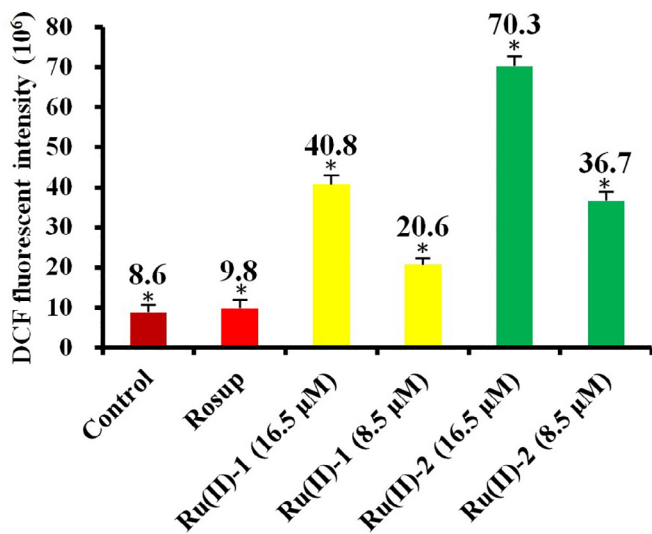


Fig. 7. The DCF fluorescent intensity was determined after HepG-2 cells treated with different concentration of the complexes for 24 h.

Ru(II)-1 and **Ru(II)-2**, the fluorescent intensities are 40.8 and 70.3, respectively. Compared the complexes with the control, the fluorescent intensities of DCF grow 4.74 and 8.17 times than the original. Unsurprisingly, the level of ROS shows a concentration-dependent manner.

We also measured intracellular superoxide anion $\text{O}_2^{\cdot-}$ levels of complexes treated HepG-2 cells using a fluorescent probe, dihydroethidium (DHE). The non-fluorescent DHE could penetrate cells freely and interact with $\text{O}_2^{\cdot-}$ to form the membrane-impermeant ethidium cation, which becomes fluorescent upon intercalating DNA, thus the fluorescence intensity of ethidium-DNA can demonstrate the level of intracellular $\text{O}_2^{\cdot-}$ [47]. As shown in Fig. 8, in the control (a), feeble red fluorescence was detected. After HepG-2

cells were exposed to 8.5 μM of **Ru(II)-1** (b) and **Ru(II)-2** (c) for 24 hour, obvious red fluorescence was observed, indicating that the complexes can enhance intracellular superoxide anion levels. To compare the effect of the **Ru(II)-1** and **Ru(II)-2** on superoxide anion levels, the fluorescent intensity was tested by ImageXpress Micro XLS system. As shown in Fig. 9, the red fluorescence intensity follows the order of **Ru(II)-2** > **Ru(II)-1**.

Subsequently, DAF-FM DA was used as a fluorescent indicator of intracellular nitric oxide (NO). After entering into the cells, this cell membrane permeable probe was hydrolyzed and then was able to react with NO to generate strong green fluorescence.[48] As show in Fig. 10, treatment of HepG-2 cells (a) with 8.5 μM of **Ru(II)-1** (b)

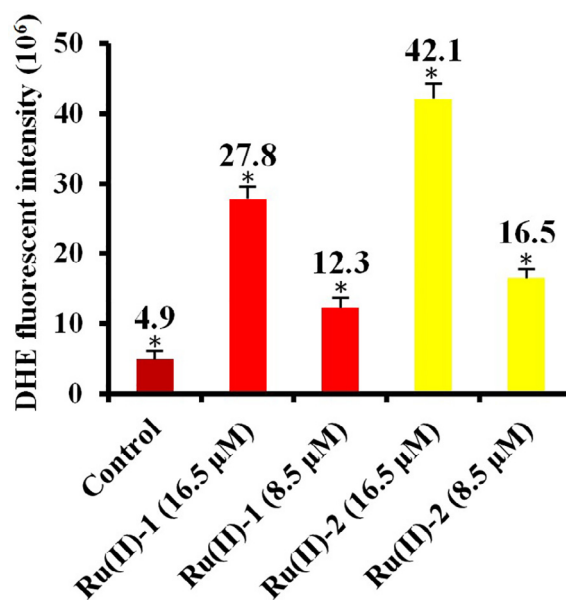


Fig. 9. The DHE fluorescent intensity was determined after HepG-2 cells treated with different concentration of the complexes for 24 h.

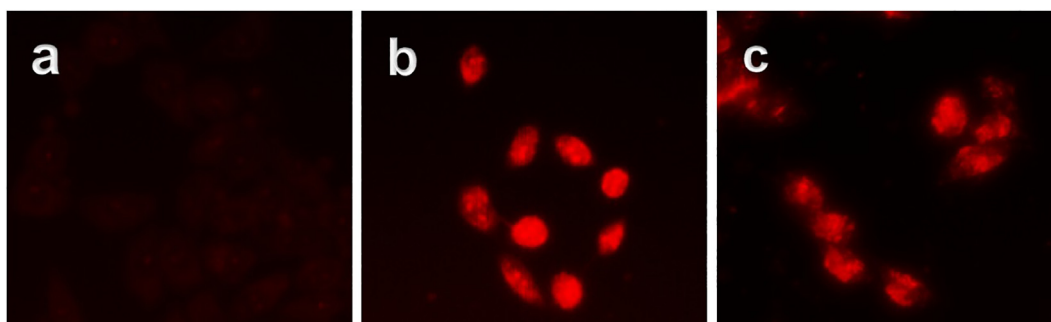


Fig. 8. The superoxide anion level was assayed after 24 h of HepG-2 cells (a) with 8.5 μM of **Ru(II)-1** (b) and **Ru(II)-2** (c) and the cells were stained with DHE.

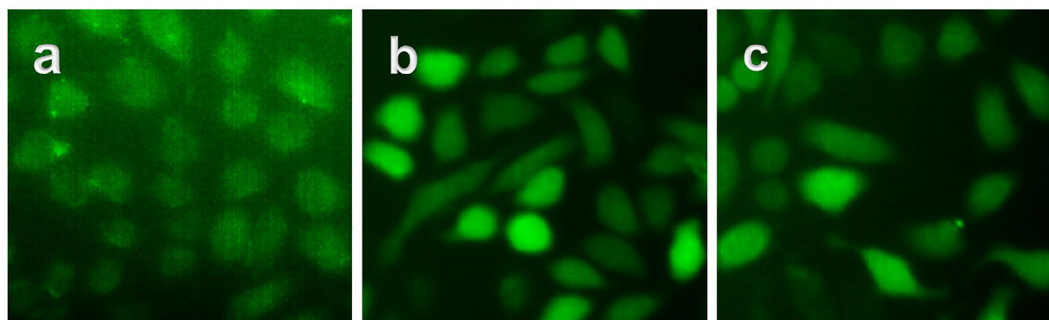


Fig. 10. The intracellular NO levels were detected after HepG-2 cells (a) were exposed to 8.5 μM of **Ru(II)-1** (b) and **Ru(II)-2** (c) for 24 h.

and **Ru(II)-2** (c) for 24 h resulted in an increase of green fluorescence. To quantitatively the effect of **Ru(II)-1** and **Ru(II)-2** on intracellular NO levels, the fluorescent intensity was tested by ImageXpress Micro XLS system. As shown in Fig. 11, in the control, the fluorescent intensity is 3.7. Compared **Ru(II)-1** (16.5 μM) and **Ru(II)-2** (16.5 μM) with the control, the fluorescent intensities

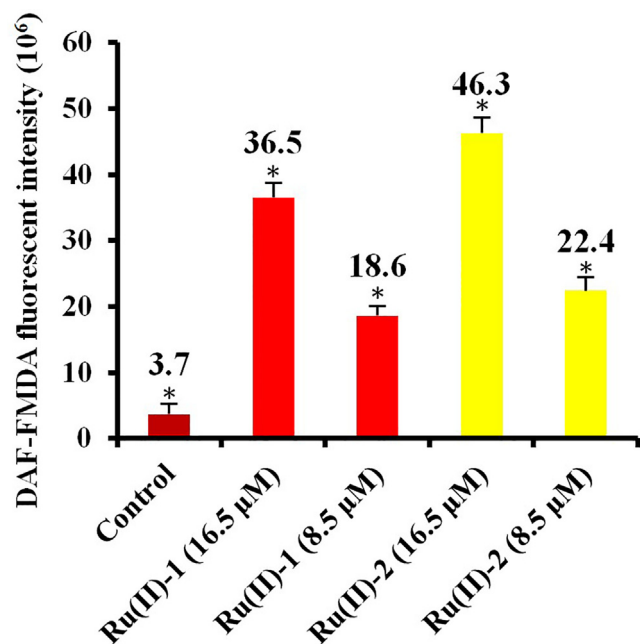


Fig. 11. The DAF-FM DA fluorescent intensity induced by the complexes was determined by ImageXpress Micro XLS system. $^*P < 0.05$ represents significant differences compared with control.

grow 9.86 and 12.51 times than the control. Furthermore, the level of NO shows a concentration-dependent manner.

3.5. Transwell cell migration and invasion assay

The migration and invasion are the significant factors in the process of tumor metastasis [49]. **Ru(II)-1** and **Ru(II)-2** can induce apoptosis and effectively inhibit the HepG-2 cells proliferation, which stimulates us to explore the effects of the complexes on inhibiting cell invasion [50]. Consequently, cellular migration was detected by determining the ability of cells to migrate through a transwell membrane using the Boyden chamber invasion assay [51]. As shown in Fig. 12, HepG-2 cells (a) were treated with 8.5 μM of **Ru(II)-1** (b) and **Ru(II)-2** (c) for 24 h, the number of cell invasion decreases. In addition, the percentage of Ru(II) complexes inhibiting the cell invasion is calculated in Fig. 13. HepG-2 cells treated with different concentrations of **Ru(II)-1** and **Ru(II)-2** showed reduced cell migration from 37.9% to 75.2% as compared to cells treated with vehicle control. These observations indicated that **Ru(II)-1** and **Ru(II)-2** played a crucial role in the inhibition of HepG-2 migration.

3.6. Cell cycle arrest studies

The proliferation inhibition or death of cells is the result of apoptosis, cell cycle arrest or a combined action of both [52]. Therefore, the ability of the ruthenium(II) complexes to arrest cell cycle was studied. As shown in Fig. 14, in the control (HepG-2), the percentage in the cell cycle at S phase is 22.11%. The treatment of HepG-2 cells with 8.5 μM of **Ru(II)-1** and **Ru(II)-2** for 24 h resulted in an increase of 20.31% and 20.83% in the cells at S phase, respectively, at the same time, a reduction of 26.96% and 25.44% in the cell at G2/M phase compared with the control were discovered. The results revealed a cell cycle arrest induced by the complexes at the S phase in HepG-2 cells.

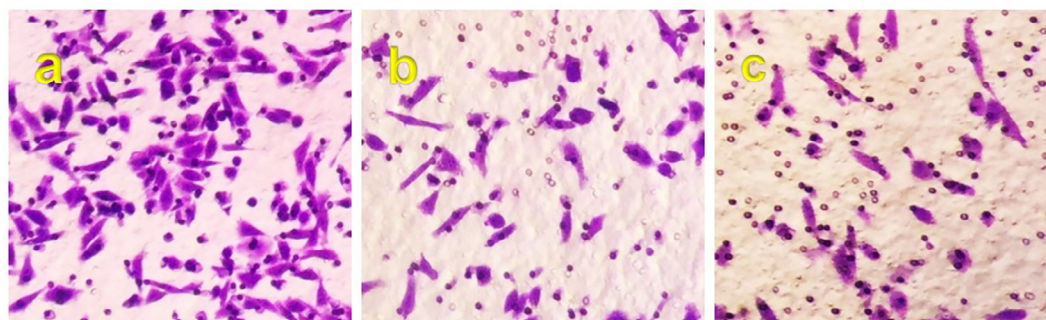


Fig. 12. Microscope images of invading HepG-2 cells (a) induced by 8.5 μM of **Ru(II)-1** (b) and **Ru(II)-2** (c) for 24 h.

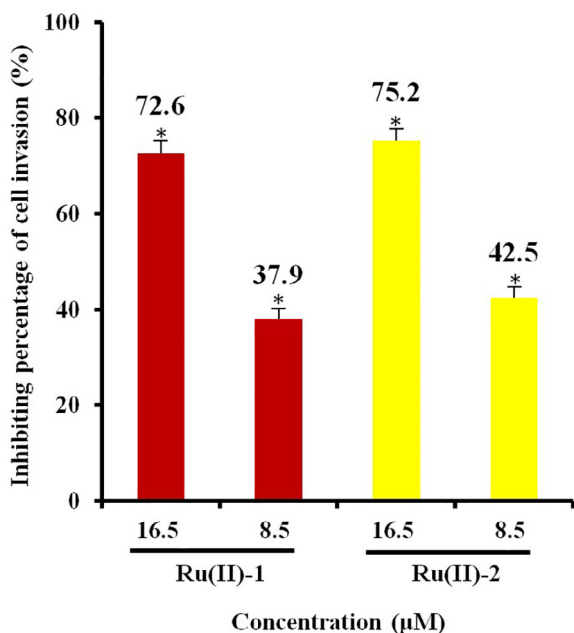


Fig. 13. Percentage of inhibiting invasion of HepG-2 cells induced by different concentration of **Ru(II)-1** and **Ru(II)-2** for 24 h. * $P < 0.05$ represents significant differences compared with control.

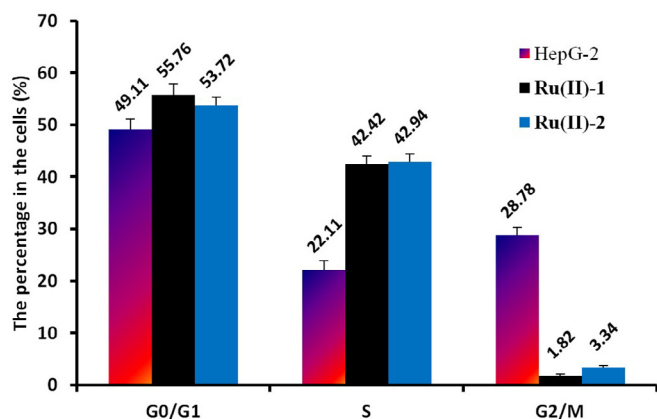


Fig. 14. The cell cycle arrest in HepG-2 cells exposed to 8.5 µM of complexes **Ru(II)-1** and **Ru(II)-2** for 24 h.

3.7. Complexes-CT DNA binding studies

Electronic absorption spectroscopy is the effective method to study the interaction of metal complexes with DNA [38]. The absorption spectra of complexes **Ru(II)-1** and **Ru(II)-2** consist of two or three resolved bands in the range 200–600 nm [53]. Absorption bands below 300 nm are caused by intraligand (IL) transition. At 320–350 nm (high energy), the spectra display a large change band, corresponding to ETPIP $\rightarrow \pi^*$ and $\pi \rightarrow \pi^*$ transitions. The spectra show a strong MLCT band at 466–468 nm contributed to overlap the Ru($d\pi$) \rightarrow ETPIP(π^*) and Ru($d\pi$) \rightarrow bpy(π^*) or phen(π^*) [54]. Fig. S1 shows spectra obtained at increasing amounts of CT DNA to **Ru(II)-1** (5.0 µM) and **Ru(II)-2** (5.0 µM) (see the Supporting Information for details). With increasing the concentration of CT DNA, the MLCT transition bands of **Ru(II)-1** at 468 nm and **Ru(II)-2** at 466 nm exhibit obvious hypochromism of about 24.3% and 25.7% and bathochromism of 5 and 4 nm, respectively. The values of K_b are $6.83 \times 10^4 \text{ M}^{-1}$ and $1.00 \times 10^5 \text{ M}^{-1}$ for the complexes **Ru(II)-1** and **Ru(II)-2**, respectively, which were less than that of the

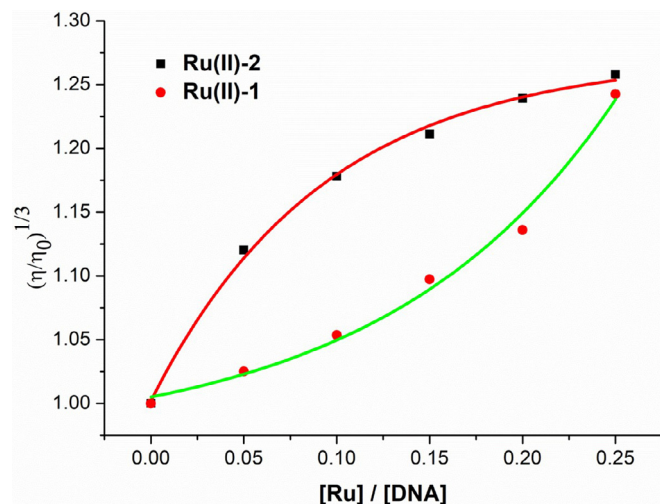


Fig. 15. The effect of increasing the amounts of the **Ru(II)-1** and **Ru(II)-2** on the relative viscosity of CT DNA at 25 (± 0.1) °C. [DNA] = 0.25 mM.

classical intercalator EB ($1.4 \times 10^6 \text{ M}^{-1}$) [55], but were higher than that of complexes [Ru(dmp)₂(maip)](ClO₄)₂ (maip = 2-(3-amino-phenyl)-imidazo[4,5-f][1,10]phenanthroline, $3.23 \times 10^4 \text{ M}^{-1}$) [56], and [Ru(dmb)₂(BFIP)]²⁺ (BFIP = 2-benzo[*b*]furan-2-yl-1*H*-imidazo[4,5-f][1,10]phenanthroline, $3.2 \times 10^4 \text{ M}^{-1}$) [57].

The emission intensities of the **Ru(II)-1** and **Ru(II)-2** from their MLCT excited states upon excitation at 468 and 466 nm were found to depend on CT DNA concentration [58]. The luminescence spectra of complexes **Ru(II)-1** and **Ru(II)-2** in the presence of increasing amounts of CT DNA in Tris buffer are shown in Fig. 2S (see the Supporting Information for details). With the addition of DNA, the emission intensities of desired complexes **Ru(II)-1** and **Ru(II)-2** grow to 1.42 and 1.43 times larger than the original, respectively. This indicates that **Ru(II)-1** and **Ru(II)-2** can strongly interact with CT DNA, and the complexes can be protected efficiently by the hydrophobic environment inside the CT DNA helix.

In the past few decades considerable progress has been made to evaluate transition metal complexes as structural probes of DNA. A series of analytical measures developed to evidence metal complexes-DNA interactions [59]. To further verify the modes of binding of complexes **Ru(II)-1** and **Ru(II)-2** to CT DNA, viscosity measurements of DNA solutions were carried out in the presence and absence of these complexes. The viscosity of DNA is sensitive to length changes and is considered as the least equivocal and the most significant clues of the DNA binding mode in solution [60]. The changes in the viscosity of CT DNA solution induced by complexes **Ru(II)-1** and **Ru(II)-2** are shown in Fig. 15. Upon increasing the concentration of complexes **Ru(II)-1** and **Ru(II)-2**, the relative viscosity of CT DNA increased obviously. These results suggest that the target complexes bind CT DNA through a classical intercalation model. The increased extent of viscosity depending on its DNA binding strength follow the order of **Ru(II)-2** > **Ru(II)-1**, which is consistent with that detected in electronic absorption titration and luminescence spectra.

4. Conclusions

Two ruthenium(II) polypyridyl complexes [Ru(bpy)₂(ETPIP)](ClO₄)₂ (**Ru(II)-1**) and [Ru(phen)₂(ETPIP)](ClO₄)₂ (**Ru(II)-2**) were synthesized and well characterized. The complexes-CT DNA binding studies imply that the complexes **Ru(II)-1** and **Ru(II)-2** interact with CT DNA via intercalative mode. Moreover, all the complexes

displayed excellent anticancer activity toward HepG-2 cells. AO/EB and Annex V/PI double staining studies showed that the complexes could induce the apoptosis of HepG-2 cells. The location studies demonstrate that the desired ruthenium(II) polypyridyl complexes could arrive the cytoplasm through the cell membrane and accumulate in the mitochondria. Additionally, these Ru(II) complexes can obviously inhibit cell invasion in HepG-2 cells. The cell cycle arrest studies reveal that complexes **Ru(II)-1** and **Ru(II)-2** induce cell cycle arrest of HepG-2 cells at S phase. Further anticancer mechanistic studies found that both the decrease of the mitochondrial membrane potential and increase of ROS contents were all related to the apoptosis of HepG-2 cells. Consequently, the complexes **Ru(II)-1** and **Ru(II)-2** induced apoptosis of the HepG-2 cells through a ROS-mediated mitochondrial dysfunction pathway. This work will be of helpful for further understanding the DNA binding and synthesizing novel ruthenium(II) polypyridyl complexes as potent antitumor agents.

Acknowledgements

This work was supported by the Ph. D. Scientific Research Foundation of Guilin University of Technology.

Appendix A. Supplementary data

Supplementary data to this article can be found online at <https://doi.org/10.1016/j.poly.2019.05.017>.

References

- [1] B. Rosenberg, L. VanCamp, J.E. Trosko, V.H. Mansour, *Nature* 222 (1969) 385.
- [2] S. Dilruba, G.V. Kalayda, *Cancer Chemother. Pharmacol.* 77 (2016) 1103.
- [3] I. Ott, R. Gust, *Arch. Pharm. Chem. Life Sci.* 340 (2007) 117.
- [4] L.R. Kelland, F.J. Barnard, I.G. Evans, B.A. Murrer, B.R.C. Theobald, S.B. Wyer, P. M. Goddard, M. Jones, M. Valenti, A. Bryant, P.M. Rogers, K.R. Harrap, *J. Med. Chem.* 38 (1995) 3016.
- [5] F.P. Intini, J. Zajac, V. Novohradské, T. Saltarella, C. Pacifico, V. Brabec, G. Natile, J. Kasparkova, *Inorg. Chem.* 56 (2017) 1483.
- [6] C.M. Clavel, E. Paunescu, P. Nowak-Sliwinska, A.W. Griffioen, R. Scopelliti, P.J. Dyson, *J. Med. Chem.* 58 (2015) 3356.
- [7] S. Page, R. Wheeler, *Educ. Chem.* (2012) 26.
- [8] A. Leonidova, G. Gasser, *ACS. Chem Biol.* 9 (2014) 2180.
- [9] Y.L. Yang, L.H. Guo, Z.Z. Tian, Y.T. Gong, H.M. Zheng, S.M. Zhang, Z.S. Xu, X.X. Ge, Z. Liu, *Inorg. Chem.* 57 (2018) 11087.
- [10] J. Sun, W.X. Chen, X.D. Song, S.F. He, J.X. Chen, J. Mei, X.X. Zhu, T. Wu, *Anti-Cancer Agent Med. Chem.* 18 (2018) 110.
- [11] T. Mede, M. Jäger, U.S. Schubert, *Chem. Soc. Rev.* 47 (2018) 7577.
- [12] J. Yellol, S.A. Pérez, A. Buceta, C. Yellol, A. Donaire, P. Szumlas, P.J. Bednarski, G. Makhlofi, C. Janiak, A. Esspinosa, J. Ruiz, *J. Med. Chem.* 58 (2015) 7310.
- [13] A. Castonguay, C. Doucet, M. Juhas, D. Maysinger, *J. Med. Chem.* 55 (2012) 8799.
- [14] D. Das, P. Mondal, *New J. Chem.* 39 (2015) 2515.
- [15] A. Vergara, G.D. Errico, D. Montesarchio, G. Mangiapia, L. Paduano, A. Merlino, *Inorg. Chem.* 52 (2013) 4157.
- [16] O. Dömötör, C.G. Hartinger, A.K. Bytzeck, T. Kiss, B.K. Keppler, E.A. Enyedy, *J. Biol. Inorg. Chem.* 18 (2013) 9.
- [17] J. Du, Y. Kang, Y. Zhao, W. Zheng, Y. Zhang, Y. Lin, Z.Y. Wang, Y.Y. Wang, Q. Luo, K. Wu, F.Y. Wang, *Inorg. Chem.* 55 (2016) 4595.
- [18] P. Elumalai, Y.J. Jeong, D.W. Park, D.H. Kim, H. Kim, S.C. Kang, K.W. Chi, *Dalton Trans.* 45 (2016) 6667.
- [19] T. Lazarević, A. Rilak, Ž.D. Bugarčić, Ž.D. Bugarčić, *Eur. J. Med. Chem.* 142 (2017) 8.
- [20] X. He, L. Jin, L. Tan, *Spectrochim. Acta, Part A* 135 (2015) 101.
- [21] R. Pettinari, C. Pettinari, F. Marchetti, B.W. Skelton, A.H. White, L. Bonfili, M. Cuccioli, M. Mozzicafreddo, V. Cecarini, M. Angeletti, M. Nabiss, A.M. Eleuteri, *J. Med. Chem.* 57 (2014) 4532.
- [22] D. Wan, S.-H. Lai, C.-C. Zeng, C. Zhang, B. Tang, Y.-J. Liu, *J. Inorg. Biochem.* 173 (2017) 1.
- [23] B. Tang, D. Wan, S.-H. Lai, H.-H. Yang, C. Zhang, X.-Z. Wang, C.-C. Zeng, Y.-J. Liu, *J. Inorg. Biochem.* 173 (2017) 93.
- [24] D. Wan, B. Tang, Y.J. Wang, B.H. Guo, H. Yin, Q.Y. Yi, Y.J. Liu, *Eur. J. Med. Chem.* 139 (2017) 180.
- [25] C.P. Tan, S.S. Lai, S.H. Wu, S. Hu, L.J. Zhou, Y. Chen, M.X. Wang, Y.P. Zhu, W. Lian, W. Peng, L.N. Ji, A.L. Xu, *J. Med. Chem.* 53 (2010) 7613.
- [26] A.F. Tikum, Y.J. Jeon, J.H. Lee, M.H. Park, I.Y. Bae, S.H. Kim, H.J. Lee, J. Kim, *J. Inorg. Biochem.* 180 (2018) 204.
- [27] A. Bergamo, G. Sava, *Dalton Trans.* 13 (2007) 1267.
- [28] C.G. Hartinger, M.A. Jakupec, S. Zorbas-Seifried, M. Groessl, A. Egger, W. Berger, H. Zorbas, P.J. Dyson, B.K. Keppler, *Chem. Biodiv.* 5 (2008) 2140.
- [29] L. Perdisatt, S. Moqadasi, L. O'Neill, G. Hessman, A. Ghion, M.Q.M. Warraich, A. Casey, C. O'Connor, *J. Inorg. Biochem.* 182 (2018) 71.
- [30] J. Marmur, *J. Mol. Biol.* 3 (1961) 208.
- [31] M.E. Reichmann, S.A. Rice, C.A. Thomas, P. Doty, *J. Am. Chem. Soc.* 76 (1954) 3047.
- [32] A. Wolf, G.H. Shimer, T. Meehan, *Biochemistry* 26 (1987) 6392.
- [33] J.B. Chaires, N. Dattagupta, D.M. Crothers, *Biochemistry* 21 (1982) 3933.
- [34] S. Satyanarayana, J.C. Dabrowiak, J.B. Chaires, *Biochemistry* 32 (1993) 2573.
- [35] S. Satyanarayana, J.C. Dabrowiak, J.B. Chaires, *Biochemistry* 31 (1992) 9319.
- [36] G. Cohen, H. Eisenberg, *Biopolymers* 8 (1969) 45.
- [37] T. Mosmann, *J. Immunol. Methods* 65 (1983) 55.
- [38] G.B. Jiang, X. Zheng, J.H. Yao, B.J. Han, W. Li, J. Wang, H.L. Huang, Y.J. Liu, *J. Inorg. Biochem.* 141 (2014) 170.
- [39] Y.Y. Qi, Q. Gan, Y.X. Liu, Y.H. Xiong, Z.W. Mao, X.Y. Le, *Eur. J. Med. Chem.* 154 (2018) 220.
- [40] S. Sampath, V. Veeramani, G.S. Krishnakumar, U. Sivalingam, S.L. Madurai, R. Chellan, *Biomed. Pharmacother.* 93 (2017) 296.
- [41] B. Peña, S. Saha, R. Barhoumi, R.C. Burghardt, K.R. Dunbar, *Inorg. Chem.* 57 (2018) 12777.
- [42] S.L. Zhang, J.L. Fan, S.Z. Zhang, J.Y. Wang, X.W. Wang, J.J. Du, X.J. Peng, *Chem. Commun.* 50 (2014) 14021.
- [43] J.J. Li, L.H. Guo, Z.Z. Tian, S.M. Zhang, Z.S. Xu, Y.L. Han, R.X. Li, Y. Li, Z. Liu, *Inorg. Chem.* 57 (2018) 13552.
- [44] Y.L. Yang, L.H. Guo, Z.Z. Tian, X.C. Liu, Y.T. Gong, H.M. Zheng, X.X. Ge, Z. Liu, *Chem. Asian J.* 13 (2018) 2923.
- [45] A. Armiñán, M. Palomino-Schätzlein, C. Deladriere, J.J. Arroyo-Crespo, S. Vicente-Ruiz, M.J. Vicent, A. Pineda-Lucena, *Biomaterials* 162 (2018) 144.
- [46] V. Venkatesh, R. Berrocal-Martin, C.J. Wedge, I. Romero-Canelón, C. Sanchez-Cano, J.I. Song, J.P.C. Coverdale, P.Y. Zhang, G.J. Clarkson, A. Habtemariam, S.W. Magennis, R.J. Deeth, P.J. Sadler, *Chem. Sci.* 8 (2017) 8271–8278.
- [47] H. He, D.W. Li, L.Y. Yang, L. Fu, X.J. Zhu, W.K. Wong, F.L. Jiang, Y. Liu, *Sci. Rep.* 5 (2015) 13543.
- [48] X. Zhang, Z. Guo, J. Liu, G. Tian, K. Chen, S.C. Yu, Z.J. Gu, *Sci. Bull.* 62 (2017) 985.
- [49] S.P. Yang, Y.G. Zhang, Y. Luo, B.C. Xu, Y.Q. Yao, Y.L. Deng, F.F. Yang, T.H. Ye, G. Wang, Z.Q. Cheng, Y. Zheng, Y.M. Xie, *Biomed. Pharmacother.* 62 (2017) 985.
- [50] W.Y. Zhang, Q.Y. Yi, Y.Y. Wang, F. Du, M. He, B. Tang, D. Wan, Y.J. Liu, H.L. Huang, *Eur. J. Med. Chem.* 151 (2018) 568.
- [51] F.U. Rahman, M.Z. Bhatti, A. Ali, H.Q. Duong, Y. Zhang, B. Yang, S. Koppireddi, Y. J. Lin, H. Wang, Z.T. Li, D.W. Zhang, *Eur. J. Med. Chem.* 143 (2018) 1039.
- [52] Y. Zhang, P.C. Hu, P. Cai, G.Z. Cheng, *RSC Adv.* 5 (2015) 11591.
- [53] P.U. Maheswari, M. Palaniandavar, *J. Inorg. Biochem.* 98 (2004) 119.
- [54] D. Lazi Dejanč, A. Arsenijević, R. Puchta, Ž.D. Bugarčić, A. Rilak, *Dalton Trans.* 45 (2016) 4633–4646.
- [55] X.B. Fu, Z.H. Lin, H.F. Liu, X.Y. Le, *Spectrochim. Acta, Part A* 122 (2014) 22.
- [56] C.H. Zeng, Y.J. Liu, Z.Z. Li, Z.H. Liang, H.L. Huang, F.H. Wu, *Transition Met. Chem.* 35 (2010) 731.
- [57] K.A. Kumar, K.L. Reddy, S. Satyanarayana, *J. Coord. Chem.* 63 (2010) 3676.
- [58] A. Srishailama, Y.P. Kumar, P.V. Reddy, N. Nambigari, U. Vuruputuri, S.S. Singhc, S. Satyanarayana, *J. Photochem. Photobiol. B Biol.* 132 (2014) 111.
- [59] C.S. Devi, B. Thulasiram, S. Satyanarayana, P. Nagababu, *J. Fluoresc.* 27 (2017) 2119.
- [60] M.M. Milutinović, A. Rilak, I. Bratsos, O. Klisurić, M. Vraneš, N. Gligorijević, S. Radulović, Ž.D. Bugarčić, *J. Inorg. Biochem.* 169 (2017) 1.